

Cite this: *Dalton Trans.*, 2019, **48**,
5327

Enhanced Néel temperature in EuSnP under pressure†

Xin Gui,^a Gregory J. Finkelstein,^b David E. Graf,^c Kaya Wei,^c Dongzhou Zhang,^b Ryan E. Baumbach,^{c,d} Przemyslaw Dera^b and Weiwei Xie^{*,a}

We present the combined results of single crystal X-ray diffraction, physical properties characterization, and theoretical assessment of EuSnP under high pressure. Single crystals of EuSnP prepared using Sn self-flux crystallize in the tetragonal NbCrN-type crystal structure (S.G. $P4/nmm$) at ambient pressure. Previous studies have shown that for Eu ions, seven unpaired electrons impart a 2+ oxidation state. Assuming the oxidation states of Eu to be +2 and P to be -3, each Sn will donate one electron, with one p valence electron left for forming a weak Sn–Sn bond. According to the high-pressure single crystal X-ray diffraction measurements, no structural phase transition was observed up to ~6.2 GPa. Temperature-dependent resistivity measurements up to 2.15 GPa on single crystals indicate that the phase-transition temperature occurring at the Néel temperature (T_N) is significantly enhanced under high pressure. The robust crystallography and enhanced antiferromagnetic transition temperatures can be rationalized by the electronic structure calculations and chemical bonding analysis. The increasing Eu–P bonding interaction is consistent with the lattice parameter changing and enhanced T_N . Moreover, the molecular orbital diagram shows that the weak Sn–Sn bond can be squeezed under pressure, acting as a compression buffer to stabilize the structure.

Received 30th January 2019,
Accepted 22nd March 2019

DOI: 10.1039/c9dt00449a

rsc.li/dalton

Introduction

The mystery of the atom is revealed upon tuning of the relative strengths of characteristic energy scales, including electronic hybridization and magnetic exchange, which combine to produce novel phenomena that include structural and magnetic instabilities. There are a wide variety of intriguing examples within this paradigm, such as the iron-based pnictides and chalcogenides, which exhibit intertwined magnetic and structural instabilities, as well as high-temperature superconductivity. Indeed, this close relationship between magnetic, structural, and other types of order is a prominent feature in many different classes of quantum materials.^{1–5} While these materials show great complexity, the atomic size appears to be a central concept and applied pressure has frequently been used to probe its role. For instance, the space requirements of atoms are key in determining structural stability, chemical reactivity, and magnetism of compounds spanning from simple

molecules to solid-state materials. Moreover, atomic or ionic radius is the primary consideration in evaluating the compressibility of an element.⁶ Particularly intriguing examples are the divalent Eu and Yb elements, with half-filled and fully-filled 4f orbitals respectively, which have significantly larger molecular volumes than other rare earth elements.^{7–10} Both theoretical and experimental studies have shown that sufficiently large pressures have the effect of varying their f-electron valences, resulting in changes in structural, thermodynamic, and electronic properties: *e.g.*, superconductivity is induced in Eu with $T_c \sim 2$ K at ~80 GPa.¹¹ While the concept of atomic space requirement is clearly important, especially from the phenomenological viewpoint, the effect of atomic size on phase stability is still difficult to extract from quantum-mechanical calculations. This makes it difficult to use a calculation-driven approach to design systems that harness the benefits of magnetic and structural instabilities. To address this challenge, a novel approach to chemical-pressure analysis was recently proposed, which provides a quantitative theoretical interpretation about size effects on structural stability.^{12–14} Following the discussion by Fredrickson *et al.*^{12–14} and Guo *et al.*,¹⁵ we use the chemical picture of bonding interactions to understand the physical properties of solid-state materials under high pressure.

Herein, we focus on the previously reported antiferromagnetic EuSnP, which has a structure that is isotopic with superconducting SrSnP.¹⁵ EuSnP crystallizes in the primitive

^aDepartment of Chemistry, Louisiana State University, Baton Rouge, LA, USA 70803.
E-mail: weiweix@lsu.edu

^bHawai'i Institute of Geophysics and Planetology, University of Hawai'i at Manoa, Honolulu, HI, USA 96822

^cNational High Magnetic Field Laboratory, Tallahassee, FL, USA 32306

^dDepartment of Physics, Florida State University, Tallahassee, FL, USA 32306

†Electronic supplementary information (ESI) available. See DOI: 10.1039/c9dt00449a

tetragonal structure with six atoms in each unit cell, and Eu–Sn–P and P–Sn–Eu linear chains along the *c*-axis. Similar to SrSnP, the Eu and P in EuSnP have oxidation states of 2+ and 3–, respectively, leaving each Sn with three valence electrons ($5s^25p^1$). Moreover, the nets of puckered Sn–Sn rings indicate that there is weak bonding between Sn and Sn (as shown in Fig. 1(A)). Since phosphorus is more electronegative, there are at most three electrons left on Sn atom after bonding with P atom. Thus, three electrons should be bonded with four Sn atoms nearby which leads to an electron-deficient environment and longer Sn–Sn bond length. The antiferromagnetism and its transition temperature were confirmed and further explored by Payne and Fujiwara through the magnetic, electric resistivity and heat capacity measurements.^{16,18} Another interesting question arises: can the electron-deficient bonds on Sn–Sn accept the electron from Eu^{2+} and prompt the transition from divalent to trivalent on Eu under high pressure? To address these questions, we performed a systematic study through single crystal X-ray struc-

tural characterization, electrical transport, and theoretical electronic structures of EuSnP under high pressure. The crystal structure of EuSnP remains unchanged up to ~ 6.2 GPa and the Néel temperature that is detected in electrical transport measurements strongly increases to 33.6 K at 2.15 GPa from the ambient pressure value of $T_N = 20$ K. The chemical bonding analysis shows that the Eu–P bonding interaction is strongly enhanced, while the Sn–P bonding interaction is heavily reduced under high pressure. The weak bond between Sn–Sn is slightly affected, which acts as the “pressure buffer” to stabilize the crystal structure.

Results & discussion

Crystal structure of EuSnP under various pressures

According to the results of single crystal X-ray diffraction, the plate-like crystals adopt NbCrN structure type with the space

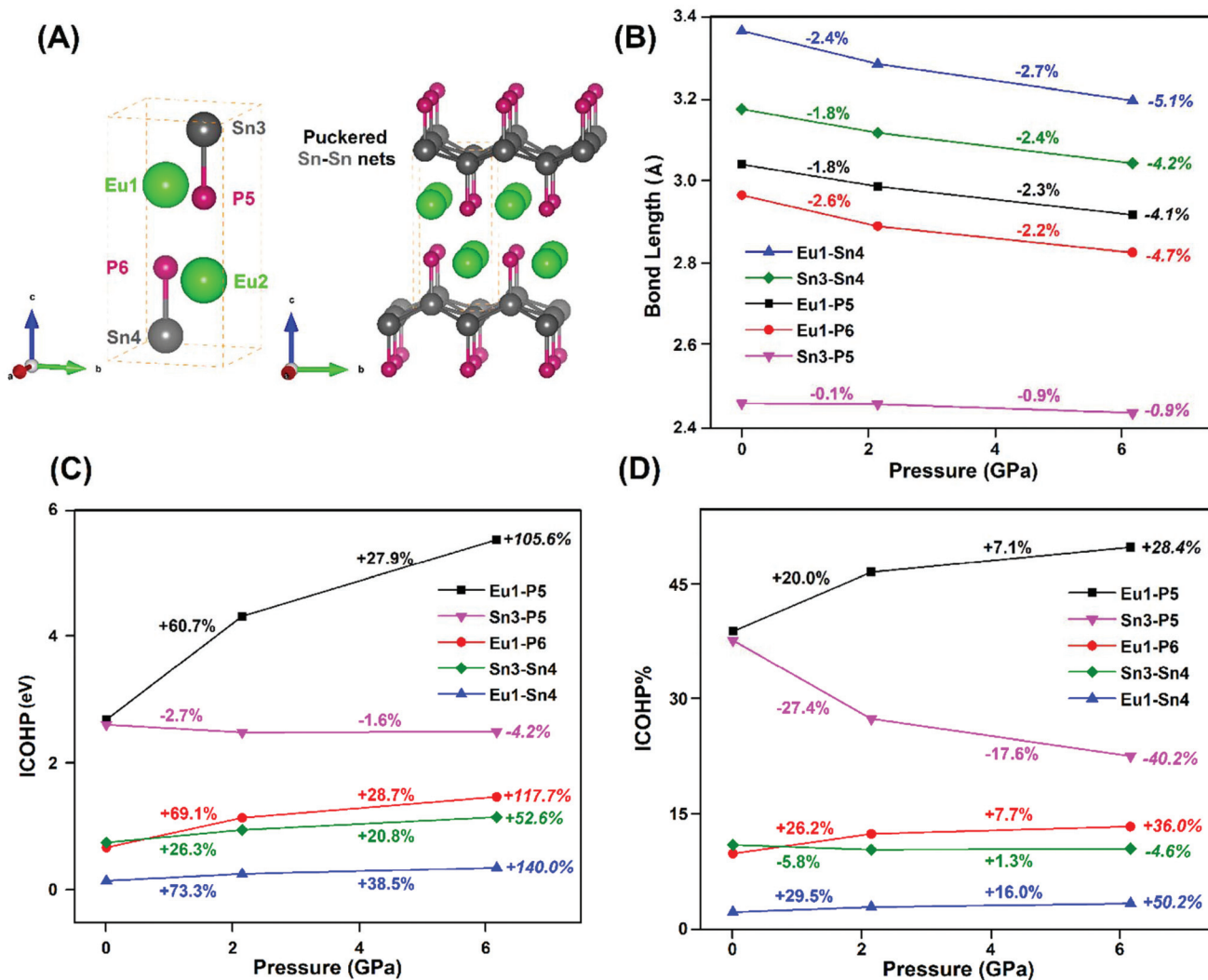


Fig. 1 (A). (Left) Crystal structure of EuSnP (green, grey, and red balls represent Eu, Sn and P, respectively). (Right) Puckered Sn–Sn nets in EuSnP. (B). Trend plot for typical bond lengths in EuSnP under pressures. (C). Integrated Crystal Orbital Hamiltonian Population (ICOHP) trend under pressures for critical atomic interactions. (D). Percentage of ICOHP changes with pressure in EuSnP.

group, $P4/nmm$, which is consistent with the reported one.¹⁶ To determine the phase purity of EuSnP single crystals, powder X-ray diffraction (PXRD) was performed with Rietveld fitting on the pattern, as shown in Fig. S1.† The PXRD pattern clearly shows a nearly pure phase, which is fitted well with the calculated pattern generated from the single crystal structure. No phase transition was observed within the pressure range we achieved (≤ 6.18 GPa). The results of single crystal X-ray diffraction data under different pressures including atomic positions, site occupancies, and isotropic displacement parameters are shown in Tables 1 and 2. The lattice parameters obtained at ambient pressure (AP) is larger than the previous reported, which is reasonable due to the difference of experimental temperatures, 293 K for our measurement and 130 K for the reported one. Lattice parameters of a and c decrease under higher pressures. The crystal structure is shown in Fig. 1(A). To better describe the bonding interaction in the following paragraphs, we marked each atom with different labels.

Bond lengths changes under various pressures

The five key atomic interactions of EuSnP and their percent changes are listed in Table S1.† The trend of bond length changes is also plotted in Fig. 1(B). All five key bond lengths decrease with pressure. Moreover, when the pressure is raised to 6.18 GPa, the bonds along c -axis decrease more than the bonds along ab -plane (-5.05% for Eu1–Sn4 & -4.72% for Eu1–P6 vs. -4.16% for Sn3–Sn4 & -4.04% for Eu1–P5), even though the decreasing of a (-4.12%) is more than that of c (-3.77%). Thus, it has been shown that more space is available along ab -plane at ambient pressure, but bonds along c -axis are more relaxing except Sn3–P5 bond, which is only 0.94% shorter at 6.18 GPa. This is due to the fact that the sum of atomic radius of Sn and P is 2.45 Å which is similar with the bond length under ambient pressure which makes it difficult to be compressed under high pressure.

Table 1 Crystallographic data obtained from single crystal X-ray diffraction of EuSnP at 293(2) K under various pressures. (AP: ambient pressure)

Pressure (GPa)	AP	2.15	6.18
Space group; Z	$P4/nmm$; 2	$P4/nmm$; 2	$P4/nmm$; 2
a (Å)	4.301 (1)	4.2229 (6)	4.1239 (6)
c (Å)	8.790 (2)	8.631 (2)	8.459 (2)
V (Å ³)	162.58 (6)	153.92 (5)	143.86 (5)
Extinction coefficient	0.119 (5)	0.000 (5)	0.001 (2)
θ range (deg)	2.317–33.211	2.360–38.971	4.820–37.798
No. reflections; R_{int}	1596; 0.0332	703; 0.0956	302; 0.0789
No. independent reflections	215	161	77
No. parameters	10	10	10
R_1 ; ωR_2 (all I)	0.0164; 0.0363	0.0544; 0.1666	0.0264; 0.0699
Goodness of fit	1.272	1.315	1.348
Diffraction peak and hole ($e^- \text{Å}^{-3}$)	1.468; -1.391	4.304; -4.470	1.181; -0.831

Table 2 Atomic coordinates and equivalent isotropic displacement parameters of EuSnP system under different pressures (U_{eq} is defined as one-third of the trace of the orthogonalized U_{ij} tensor (Å²))

Pressure	Atom	Wyckoff.	Occ.	x	y	z	U_{eq}
AP	Eu	2c	1	$\frac{1}{4}$	$\frac{1}{4}$	0.8309 (0)	0.0093 (1)
	Sn	2c	1	$\frac{1}{4}$	$\frac{1}{4}$	0.4479 (1)	0.0141 (2)
	P	2c	1	$\frac{1}{4}$	$\frac{1}{4}$	0.1683 (2)	0.0093 (3)
2.14 GPa	Eu	2c	1	$\frac{1}{4}$	$\frac{1}{4}$	0.6713 (2)	0.0126 (8)
	Sn	2c	1	$\frac{1}{4}$	$\frac{1}{4}$	0.0520 (3)	0.0201 (9)
	P	2c	1	$\frac{1}{4}$	$\frac{1}{4}$	0.336 (1)	0.006 (2)
6.18 GPa	Eu	2c	1	$\frac{1}{4}$	$\frac{1}{4}$	0.6736 (1)	0.0106 (6)
	Sn	2c	1	$\frac{1}{4}$	$\frac{1}{4}$	0.0516 (2)	0.0178 (7)
	P	2c	1	$\frac{1}{4}$	$\frac{1}{4}$	0.3395 (6)	0.010 (2)

Bonding interactions of EuSnP under various pressures

The Crystal Orbital Hamiltonian Population (COHP) calculation of critical atomic interactions in EuSnP is plotted in Fig. 2. Bond lengths, integrated COHP (–ICOHP), –ICOHP% and their percentage changing are listed in Tables S2–S4 in the ESI.† The trends of –ICOHP and –ICOHP% are shown in Fig. 1(C) & (D).

Eu1–P5 bond

According to Fig. 1(C), the –ICOHP of Eu1–P5 increases sharply at 6.18 GPa ($\sim +105.6\%$). This may be due to the shrinkage of bond length of Eu1–P5 under pressure. As can be seen from Table S1,† its bond length is reduced to 2.918 Å from 3.041 Å (AP), which is fairly equivalent to the sum of the atomic radii of Eu and P, which is 2.85 Å. Therefore, the interaction between Eu and P here is getting stronger, thus, the bonding energy can be significantly increased.

Eu1–Sn4 bond

The –ICOHP of Eu1–Sn4 boosts the most comparing with ambient pressure ($\sim +140\%$). Furthermore, the bond length at 6.18 GPa (3.197 Å) indicates that it should be stronger bond in contrast with 3.3 Å, which is the sum of atomic radius of Eu and Sn. However, its –ICOHP% it is not in agreement with the speculation. According to previously reported EuSnP,¹⁶ the oxidation state of Eu is assigned as +2 and P is generally to be -3 , therefore each Sn will remain one p valence electron and positive oxidation state. The positive oxidation state of the Sn atom was subsequently demonstrated in the similar superconducting SrSnP.¹⁷ Thus, the reason for this conflict can be the similarity of their positive oxidation states, which ultimately leads to a weak interaction between Eu1 and Sn4.

Sn3–P5, Eu1–P6 and Sn3–Sn4 bonds

The most attractive part is that even though Sn3–P5 distance (2.435 Å) is shorter than the sum of atomic radius of Sn and P (2.45 Å), its –ICOHP still decreases at 6.18 GPa ($\sim -4.2\%$). Possible reasons can be found in our previous paper describing superconducting SrSnP, where we claim that in Sn–P–Sr–Sn linear chain, the strong Sr–P bonding orbital overlaps with antibonding orbital of Sn–P pair, which will weaken Sn–P

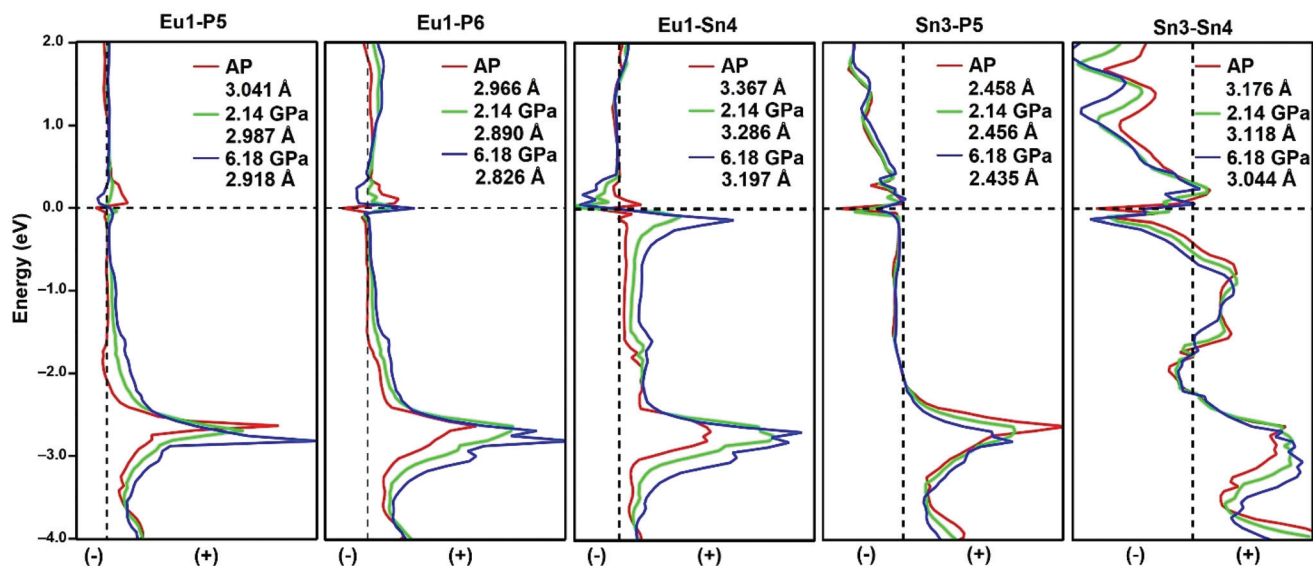


Fig. 2 Crystal Orbital Hamiltonian Population (COHP) calculation for atomic interactions in EuSnP under various pressures where (-) indicates anti-bonding interaction and (+) shows bonding interaction.

bonding interaction. Similarly, in EuSnP, even if the length of the Sn3–P5 bond is decreased, the shrinkage of Eu1–P6 bond and the increasing in -ICOHP are remarkable, which is able to overlap the influence of decreasing of Sn3–P5 bond length. Moreover, the -ICOHP of Sn3–Sn4 also increases with pressure, but as the -ICOHP of Eu1–P6 increases significantly, its -ICOHP% decreases.

Electrical resistivity under various pressures

Fig. 3 displays the temperature dependence of the electrical resistivity $\rho(T)$ of EuSnP at temperatures $T = 2$ –50 K and several pressures up to 2.15 GPa. At elevated temperatures ($T > T_N$), all of the curves exhibit metallic behavior and are similar to each other, as shown in Fig. S2.† The phase transi-

sition to the antiferromagnetic state is seen in $\rho(T)$ as a sharp decrease which represents the removal of spin disorder scattering upon entering the ordered state. The transition temperature T_N can be defined from the sharp peak in heat capacity measurement (Fig. S3†) and rapidly increases with increasing pressure. Above T_N , the pressure dependence of resistivity is relatively small, and the temperature-dependent resistivity is the same for all pressures. The temperature-dependence is the same for temperature well below T_N . The Eu–Eu atomic distance decreases slightly from 4.24 Å at ambient pressure to 4.20 Å at 2.15 GPa. These results suggest that the antiferromagnetic interactions between the Eu atoms mediated by conduction electrons are strengthened upon reducing the interatomic distances by pressure. Based on the above high-pressure

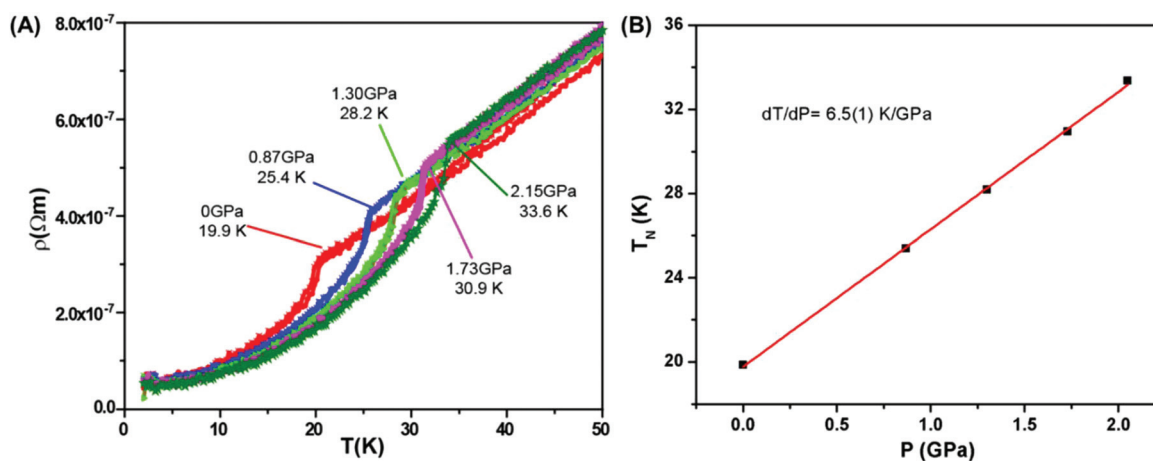


Fig. 3 (A) Temperature dependence of resistivity $\rho(T)$ at various pressures up to 2.15 GPa with magnified temperature ranging from 2 to 50 K. (B) Pressure-dependent magnetic ordering transition temperatures with $dT/dP = 6.5(1)$ K GPa^{-1} with $R^2 = 0.999$.

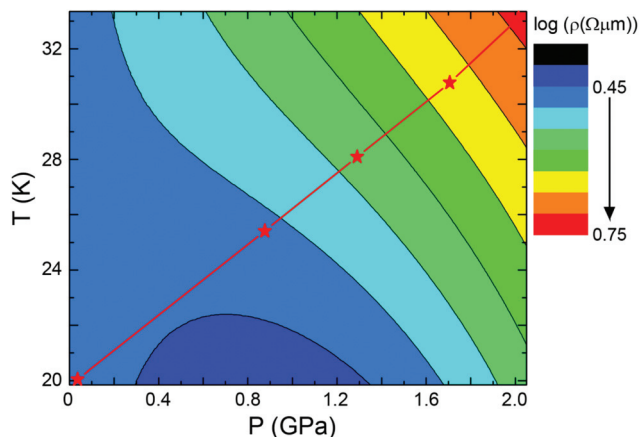


Fig. 4 Contour map in the temperature–pressure (T – P) plane for resistivity in EuSnP. The color bars at the side of the map represent the magnitude of the resistivity. The stars represent the transition temperatures at different pressures. ($0 \text{ GPa} < P < 2.15 \text{ GPa}$ and $19.9 \text{ K} < T < 33.6 \text{ K}$).

resistivity measurements, we can summarize the temperature–pressure curve for EuSnP single crystal in Fig. 4, which shows the linear behavior with $dT_N/dP = 6.5(1) \text{ K GPa}^{-1}$.

Molecular orbital (MO) calculation

Each EuSnP unit cell has 36 valence electrons totally which indicates that MO #18 can be considered as the highest occupied molecular orbital (HOMO). To visualize the change in molecular orbital #17, we moved the origin of the unit cell to $(\frac{1}{2}, \frac{1}{2}, \frac{1}{2})$ (Fig. 5A) and performed the calculation using the extended Hückel method. Other results are summarized in Fig. 5B, C & D.

As shown in Fig. 5A, MO appears around Sn and Eu atoms and, along with pressure increasing, significant bonding interaction between Eu/Sn and Sn emerges. The result is consistent with –ICOHP data that Sn3–Sn4 boosts 52.63% from ambient pressure to 6.18 GPa while Eu1–Sn4 was raised up 140% based on the original one. When it turns to Eu–P interaction, which is highlighted in COHP/–ICOHP section, Fig. 5B, C & D clearly illustrate that more bonding components occur between Eu–P–Eu–P net while pressure is getting larger. Even though a degeneracy appears between MO #17 & MO #18 under 2.15 GPa, they are still distinguishable in accordance with the relationship between MOs under other pressures. According to Fig. 3B, only phase change is observed when pressure is raised to 2.15 GPa, however, a notable difference, *i.e.*, bonding interaction, can be observed within Eu–P–Eu–P net at 6.18 GPa. In addition, phase changes also emerge less than 2.15 GPa for HOMO & LUMO, as shown in Fig. 5C & D. Clear MO images and direct interaction inside Eu–P–Eu–P net can be observed for both HOMO & LUMO at 6.18 GPa. In summary, the MO calculations provide evidence and are consistent with our observations and speculations in COHP/–ICOHP calculation that Eu–P, Eu–Sn & Sn–Sn interactions strengthen with pressure. However, Sn–P interaction can barely change; even get weaker through increasing pressure.

Conclusions

Antiferromagnetic EuSnP was studied under high pressure up to $\sim 6.2 \text{ GPa}$. No structural phase transition was detected through single crystal X-ray diffraction up to $\sim 6.2 \text{ GPa}$. The high-pressure resistivity measurements were conducted up to

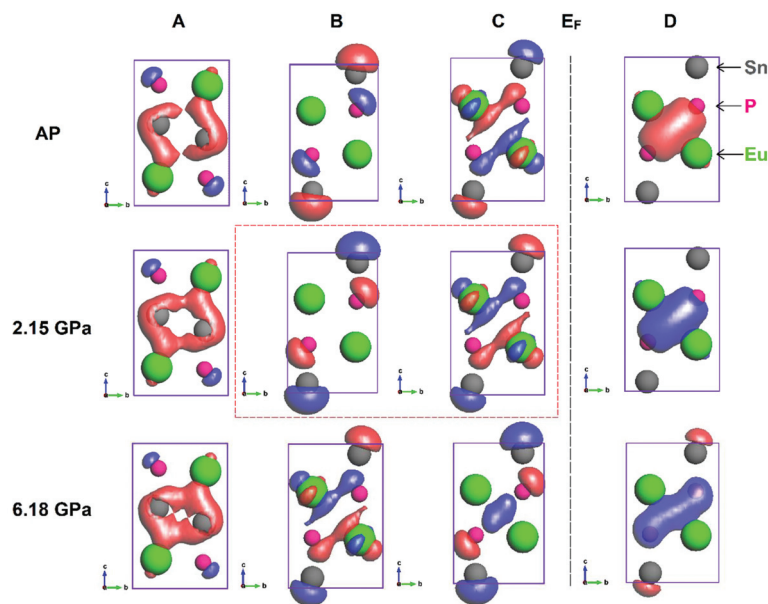


Fig. 5 Molecular Orbitals (MOs) of EuSnP under different pressures. Column A: MO #17 when moving origin from $(0, 0, 0)$ to $(\frac{1}{2}, \frac{1}{2}, \frac{1}{2})$; Column B: MO #17; Column C: MO of orbital #18 (highest occupied molecular orbital (HOMO)); Column D: MO of orbital #19 (lowest unoccupied molecular orbital (LUMO)). Green, grey and pink balls represent Eu, Sn and P atoms, respectively. Red dashed line indicates degeneracy.

2.15 GPa. The results show that the Néel temperature (T_N) in EuSnP is significantly enhanced under high pressure with $dT_N/dP = 6.5(1) \text{ K GPa}^{-1}$. The conjugated Sn–Sn square network form two-center two-electron (2c–2e) bonds can be squeezed under high pressure to stabilize the structure. The robust crystallographic and enhanced antiferromagnetic transition temperature can be rationalized by the electronic structure calculations and chemical bonding analysis. The enhanced Eu–P bonding interaction is consistent with the lattice parameter changing and increasing T_N . The high-pressure study on EuSnP will offer us an ideal platform to study the relationship between chemical bonding interactions and physical properties of solid-state materials under high pressure.

Experimental section

Single crystal growth of EuSnP

To grow single crystals of EuSnP, the same self-flux method that has been used for SrSnP was employed.¹⁷ A mixture of Eu, red phosphorus (99%, ~ 100 meshes, Beantown Chemical) and Sn granules (99.5%, Alfa Aesar), with a molar ratio of 1 : 1 : 20 were put into an alumina crucible, which was subsequently sealed into an evacuated quartz tube. The sealed tube was heated to 600 °C with a rate of 30 °C h⁻¹ and held there for 24 hours following by heating up to 1050 °C with the same rate. After annealing at 1050 °C for 24 hours, the tube was slowly cooled down to 600 °C at a rate of 3 °C h⁻¹. Plate-shaped single crystals (~0.1 × 2.5 × 2.5 mm³) of EuSnP were obtained after removing excess Sn by centrifuging.

Single crystal X-ray diffraction at ambient pressure

More than ten pieces of single crystals (~5 × 40 × 40 μm³) were tested under ambient conditions. A Bruker Apex II diffractometer equipped with Mo radiation ($\lambda_{K\alpha} = 0.71073 \text{ \AA}$) was used to determine the structure. A glycerol-protected sample was mounted on a Kapton loop and data collected at four different angles with an exposure time of 5 seconds per frame and a scanning 2θ width of 0.5°. In order to solve the crystal structure, direct methods and full-matrix least-squares on F^2 models with SHELXTL package were used.¹⁹ Bruker SMART software was employed to apply Lorentz and polarization intensity corrections.²⁰ Numerical absorption corrections using a face-indexed model were applied in XPREP.^{21,22}

Single crystal X-ray diffraction at high pressure

To guarantee the consistency, the same piece of single crystal used under ambient pressure was loaded into a diamond anvil cell (DAC) with a culet size of 300 μm and measured under high pressure. Before loading the sample, a rhenium gasket was pre-indented on DAC to a thickness of ~50 μm. The backing plates we used are tungsten carbide WC. The gasket hole (~200 μm) was produced by using laser before filling with pressure medium, which is a combination of methanol, ethanol and water with a volume ratio of 16 : 3 : 1. The sample

was placed into the gasket hole together with two small ruby spheres on opposite sides of the crystal. The pressure was indicated by the R1 ruby fluorescence line.²³ High-pressure single crystal X-ray diffraction was carried out at the experimental station 13BMC, GSECARS facility at APS, Argonne National Laboratory. The monochromatic incident beam energy is 28.6 keV and is focused to get a beam size of 12 μm (H) × 18 μm (V). MAR165 charge-coupled device (CCD) was employed as the detector. During the exposure, the DAC axis was parallel to the beam with an exposure time of 0.5 s per °. Data collection was performed at three different detector positions. A step scan with 1° rotation steps was also applied under each pressure. Two different pressure steps were approached, which are 2.15 GPa and 6.18 GPa. The GSE_ADA/RSV software package was employed to analyze the diffraction data.²⁴ Crystal structure refinement was done by using SHELXL package.¹⁹

Resistivity measurement under high pressure

The high-pressure electrical resistivity of EuSnP was measured using the standard four-probe method. The samples were pressurized using a nonmagnetic piston-cylinder clamp cell with Daphne oil as the pressure transmitting medium to ensure a hydrostatic pressure during pressurization.²⁵ The pressure was calibrated using the fluorescence of a ruby chip where one of the lines is known to shift, 0.0365 nm kBar⁻¹.²⁶ Details about the experimental setup can be found elsewhere.^{27–29} We have measured high-pressure resistivity on two EuSnP single crystals in this study, and found an excellent reproducibility for the observed results described below.

Electronic structure calculations

Tight-binding, linear muffin-tin orbital-atomic spheres approximation (TB-LMTO-ASA)

Tight-Binding, Linear Muffin-Tin Orbital-Atomic Spheres Approximation (TB-LMTO-ASA) using the Stuttgart code was utilized to draw Calculations of Crystal Orbital Hamiltonian Population (–COHP) curves.^{30–32} In this case, we set 0.05 meV as the convergence criterion and a mesh of 64 k points was used to generate all integrated values. Overlapping Wigner-Seitz (WS) spheres were applied to fill the space in ASA method.³³ We consider that in each WS sphere the symmetry of potential is isotropic while there is a combined correction on the overlapping part. The WS radii are: 2.006 Å for Eu; 1.480 Å for Sn; and 1.362 Å for P. Empty spheres are required for the calculation, and the overlap of WS spheres is limited to no larger than 16%. Eu 6s, 5d; Sn 5s, 5p; and P 3s, 3p wavefunctions were applied as the basis set for the calculations.

Molecular orbital (MO) calculation

Semi-empirical extended-Hückel-tight-binding (EHTB) methods and CAESAR packages are employed in calculating molecular orbitals of EuSnP under pressures.³⁴ The basis sets for Eu are: 6s: Hii = –7.42 eV, $\zeta_1 = 1.400$, coefficient1 = 1.0000; 6p: Hiii = –4.65 eV, $\zeta_1 = 1.400$, coefficient1 = 1.000; 5d:

Hii = -8.08 eV, $\zeta_1 = 2.753$, coefficient1 = 0.7187, $\zeta_2 = 1.267$, coefficient2 = 0.4449; 4f: Hii = -11.28 eV, $\zeta_1 = 6.907$, coefficient1 = 0.7354, $\zeta_2 = 2.639$, coefficient2 = 0.4597. For Sn: 5s: Hii = -16.16 eV, $\zeta_1 = 2.120$, coefficient1 = 1.000; 5p: Hii = -8.32 eV, $\zeta_1 = 1.820$, coefficient1 = 1.000. For P: 3s: Hii = -18.60 eV, $\zeta_1 = 1.750$, coefficient1 = 1.000; 3p: Hii = -14.00 eV, $\zeta_1 = 1.300$, coefficient1 = 1.000.

Conflicts of interest

There are no conflicts to declare.

Acknowledgements

W. X. deeply appreciates the inspiring discussion with Dr Takeshi Egami (Oak Ridge National Laboratory, University of Tennessee-Knoxville). The high-pressure single crystal X-ray measurement performed at GeoSoilEnviroCARS (The University of Chicago, Sector 13), Advanced Photon Source (APS), Argonne National Laboratory. GeoSoilEnviroCARS is supported by the National Science Foundation - Earth Sciences (EAR-1634415) and Department of Energy - GeoSciences (DE-FG02-94ER14466). Part of this research is supported by COMPRES under NSF Cooperative Agreement EAR-1661511. This research used resources of the Advanced Photon Source, a U.S. Department of Energy (DOE) Office of Science User Facility operated for the DOE Office of Science by Argonne National Laboratory under Contract No. DE-AC02-06CH11357. Magnetism and electrical transport measurements were performed at the National High Magnetic Field Laboratory, which is supported by National Science Foundation through NSF/DMR-1644779 and the State of Florida. W. X. was supported by the U.S. Department of Energy, Office of Science, Basic Energy Sciences, under EPSCoR Grant No. DE-SC0012432 with additional support from the Louisiana Board of Regents. X. G. was supported by NSF-OIA-1832967. G. F., D. Z. Z., and P. D. acknowledge support from the University of Hawaii Materials Science Consortium for Research and Education (MSCoRE). K. W. acknowledges the support of the Jack E. Crow Postdoctoral Fellowship.

References

- 1 J. Paglione and R. L. Greene, *Nat. Phys.*, 2018, **6**, 645–658.
- 2 T. Imai, K. Ahilan, F. L. Ning, T. M. McQueen and R. J. Cava, *Phys. Rev. Lett.*, 2009, **102**, 177005.
- 3 Y. Mizuguchi, F. Tomioka, S. Tsuda, T. Yamaguchi and Y. Takano, *Appl. Phys. Lett.*, 2008, **93**, 152505.
- 4 W. Wu, J. Cheng, K. Matsubayashi, P. Kong, F. Lin, C. Jin, N. Wang, Y. Uwatoko and J. Luo, *Nat. Commun.*, 2014, **5**, 5508.
- 5 K. W. Yeh, T. W. Huang, Y. L. Huang, T. K. Chen, F. C. Hsu, P. M. Wu, Y. C. Lee, Y. Y. Chu, C. L. Chen, J. Y. Luo and D. C. Yan, *EPL*, 2009, **84**, 605–609.
- 6 S. M. Clarke, M. Amsler, J. P. Walsh, T. Yu, Y. Wang, Y. Meng, S. D. Jacobsen, C. Wolverton and D. E. Freedman, *Chem. Mater.*, 2017, **29**, 5276–5285.
- 7 W. Bi, Y. Meng, R. S. Kumar, A. L. Cornelius, W. W. Tipton, R. G. Hennig, Y. Zhang, C. Chen and J. S. Schilling, *Phys. Rev. B: Condens. Matter Mater. Phys.*, 2011, **83**, 104106.
- 8 A. Jayaraman, *Rev. Mod. Phys.*, 1983, **55**, 65–108.
- 9 B. Johansson and A. Rosengren, *Phys. Rev. B: Solid State*, 1975, **11**, 2836–2857.
- 10 X. Tan, G. Fabbris, D. Haskel, A. A. Yaroslavtsev, H. Cao, C. M. Thompson, K. Kovnir, A. P. Menushenkov, R. V. Chernikov, V. O. Garlea and M. Shatruk, *J. Am. Chem. Soc.*, 2016, **138**, 2724–2731.
- 11 M. Debessai, T. Matsuoka, J. J. Hamlin, J. S. Schilling and K. Shimizu, *Phys. Rev. Lett.*, 2009, **102**, 197002.
- 12 V. M. Berns and D. C. Fredrickson, *Inorg. Chem.*, 2013, **52**, 12875–12877.
- 13 D. C. Fredrickson, S. Lee and R. Hoffmann, *Angew. Chem., Int. Ed.*, 2007, **46**, 1958–1976.
- 14 D. C. Fredrickson, *J. Am. Chem. Soc.*, 2011, **133**, 10070–10073.
- 15 K. Guo, L. Akselrud, M. Bobnar, U. Burkhardt, M. Schmidt, J. T. Zhao, U. Schwarz and Y. Grin, *Angew. Chem., Int. Ed.*, 2017, **56**, 5620–5624.
- 16 A. C. Payne, A. E. Sprauve, A. P. Holm, M. M. Olmstead, S. M. Kauzlarich and P. Klavins, *J. Alloys Compd.*, 2002, **338**, 229–234.
- 17 X. Gui, Z. Sobczak, T. R. Chang, X. Xu, A. Huang, S. Jia, H. T. Jeng, T. Klimczuk and W. Xie, *Chem. Mater.*, 2018, **30**, 6005–6013.
- 18 T. Fujiwara, Y. Saiga, T. J. Sato, M. Hedo and Y. Uwatoko, Magnetic properties of EuSnP, *Phys. B*, 2006, **378**, 1122–1123.
- 19 G. M. Sheldrick, *Acta Crystallogr., Sect. A: Found. Crystallogr.*, 2008, **64**, 112–122.
- 20 G. M. Sheldrick, *Acta Crystallogr., Sect. A: Found. Crystallogr.*, 2010, **66**, 479–485.
- 21 H. H. Paalman and C. J. Pings, *J. Appl. Phys.*, 1962, **33**, 2635–2639.
- 22 T. R. Schneider and G. M. Sheldrick, *Acta Crystallogr., Sect. D: Biol. Crystallogr.*, 2002, **58**, 1772–1779.
- 23 H. K. Mao, P. M. Bell, J. W. Shaner and D. J. Steinberg, *J. Appl. Phys.*, 1978, **49**, 3276–3283.
- 24 P. Dera, K. Zhuravlev, V. Prakapenka, M. L. Rivers, G. J. Finkelstein, O. Grubor-Urošević, O. Tschauer, S. M. Clark and R. T. Downs, *High Pressure Res.*, 2013, **33**, 466–484.
- 25 K. Murata, K. Yokogawa, H. Yoshino, S. Klotz, P. Munsch, A. Irizawa, M. Nishiyama, K. Iizuka, T. Nanba, T. Okada and Y. Shiraga, *Rev. Sci. Instrum.*, 2008, **79**, 085101.
- 26 D. D. Ragan, R. Gustavsen and D. Schiferl, *J. Appl. Phys.*, 1992, **72**, 5539–5544.

- 27 K. W. Chen, D. Graf, T. Besara, A. Gallagher, N. Kikugawa, L. Balicas, T. Siegrist, A. Shekhter and R. E. Baumbach, *Phys. Rev. B*, 2016, **93**, 045118.
- 28 O. Cyr-Choinière, D. LeBoeuf, S. Badoux, S. Dufour-Beauséjour, D. A. Bonn, W. N. Hardy, R. Liang, D. Graf, N. Doiron-Leyraud and L. Taillefer, *Phys. Rev. B*, 2018, **98**, 064513.
- 29 D. VanGennep, D. E. Jackson, D. Graf, H. Berger and J. J. Hamlin, *J. Phys.: Condens. Matter*, 2017, **29**, 295702.
- 30 R. Dronskowski and P. E. Bloechl, *J. Phys. Chem.*, 1993, **97**, 8617–8624.
- 31 O. K. Andersen and O. Jepsen, *Phys. Rev. Lett.*, 1984, **53**, 2571–2574.
- 32 O. K. Andersen, *Phys. Rev. B: Solid State*, 1975, **12**, 3060–3083.
- 33 S. M. Sze and K. K. Ng, *Physics of Semiconductor Devices*, John Wiley & Sons, New York, 2006.
- 34 R. Hoffmann, *J. Chem. Phys.*, 1963, **39**, 1397–1412.